Structural Insights into 19−Atom Pd/Pt Nanoparticles: A Computational Perspective

ARTICLE *in* THE JOURNAL OF PHYSICAL CHEMISTRY C · SEPTEMBER 2009

Impact Factor: 4.77 · DOI: 10.1021/jp904518e

6 AUTHORS, INCLUDING:

Dora Julia Borbón
Universidad de Sonora (Unison)
12 PUBLICATIONS **28** CITATIONS
SEE PROFILE

Alvaro Posada-Amarillas
Universidad de Sonora (Unison)
62 PUBLICATIONS **829** CITATIONS
SEE PROFILE

Roy L Johnston
University of Birmingham
240 PUBLICATIONS **6,569** CITATIONS
SEE PROFILE

Juan MARTIN Montejano-Carrizales
Universidad Autónoma de San Luis Potosí
88 PUBLICATIONS **904** CITATIONS
SEE PROFILE

Structural Insights into 19-Atom Pd/Pt Nanoparticles: A Computational Perspective

Dora J. Borbón-González,[†] Rafael Pacheco-Contreras,[‡] Alvaro Posada-Amarillas,[*,§] J. Christian Schön,[||] Roy L. Johnston,[⊥] and Juan Martín Montejano-Carrizales[#]

Departamento de Matemáticas, Programa de Posgrado en Ciencias (Física), and Departamento de Investigación en Física, Universidad de Sonora, Hermosillo, Sonora, México, Max Planck Institut für Festkörperforschung, Heisenbergstrasse 1, D-70569 Stuttgart, Germany, School of Chemistry, University of Birmingham, Edgbaston, B15 2TT, Birmingham, United Kingdom, and Instituto de Física, Universidad Autónoma de San Luis Potosí

Received: May 14, 2009; Revised Manuscript Received: July 15, 2009

We present a systematic study of the structural changes of 19-atom Pd_nPt_{19-n} nanoparticles as a function of composition, modeling the interatomic interactions with the many-body Gupta potential and using a genetic algorithm to obtain the lowest energy structures for all possible compositions. Topological analysis reveals that most of the structures are based on icosahedral packings and are strongly composition dependent. The pure Pd_{19} nanoparticle exhibits a double icosahedral geometry, while the Ino decahedron is the basis of the Pt_{19} cluster structure, which has a lower symmetry. Several structural motifs of the predicted lowest energy configurations are observed for bimetallic clusters in the range of compositions studied here. Six ideal structural families have been identified. Our results show that, for Pt-rich clusters, Pt atoms segregate into the core and the number of Pd−Pt bonds increases, while for Pd-rich clusters, the surface-segregated Pd atoms tend not to be nearest-neighbors. X-ray diffraction structure factors are simulated for all the predicted structures.

I. Introduction

Nanoalloys have recently become the subject of intense experimental and theoretical studies, mainly due to the potential that nanoparticles have for applications in fields such as chemistry, biology, and electronics.[1] The addition of a second metallic component increases the complexity of nanoparticles and also affords the opportunity to improve desired properties.[2] Thus, tailor-made nanoalloys have become a reality, resulting in the production of extraordinary new nanomaterials for applications in, for example, heterogeneous catalysis and biological sensing.[3−5] In particular, transition and noble metal nanoparticles have received considerable attention as a consequence of their possible applications in fields such as optics, heterogeneous catalysis, hydrogen storage, and biomedicine.[3,6−9]

Wet chemical synthesis methods are widely used in the preparation of bimetallic nanomaterials, usually starting from the reduction of metal ions to metal atoms, such as successive reduction of two metal salts.[10,11] This is an important method because it is currently used to prepare core−shell bimetallic nanoparticles, as in the catalyst nanoparticles used, for example, in hydrogen fuel-cell devices for selective CO oxidation.[12] Chemical ordering and a high surface/volume ratio are important characteristics of these types of catalysts, and, in particular, of those having Pd atoms on the nanoparticle's external shell. It has been shown that Pd catalysts are highly active and selective for the production of methanol in the CO hydrogenation reaction.[4] It has also been found that the size, morphology and atomic ordering of nanoalloys are dependent on the preparation conditions, regardless of the synthesis method. In particular, it has been shown that the calcination temperature plays a key role in the formation of Pd−Pt nanoalloys and that heat treatment and hydrogenation can change the surface composition of (for example) Pt−Ru and Pt−Rh nanoalloys.[13]

Exceptional attention has been paid to the preparation of Pd/Pt nanoparticles, mainly due to experimental studies indicating high catalytic activity, long-term stability, and good quality as catalysts for several major chemical reactions, such as hydrodechlorination of dichlorodifluoromethane and combustion of methane.[14] Bimetallic Pd/Pt nanoalloys are used in catalytic converters for the removal of CO, NO_x, and aromatic hydrocarbons for pollution control in exhaust gases,[15] essentially because these nanoalloys have proven to be better catalysts in the above-mentioned chemical reactions than monometallic catalysts, e.g., pure Pd nanoparticles.[16]

Experimental and computer simulation studies of binary transition metal (TM) nanoparticles have revealed intriguing morphological characteristics, with structural motifs ranging from noncrystalline (amorphous, icosahedral, or decahedral) to crystalline (fcc, hcp) structures.[17] Theoretical computational studies on structural characterization of nanoparticles have been performed using both first principles methods and semiempirical potentials. First principles calculations involve large computational resources, and only limited studies have been performed on nanoalloys because of the high number of permutational isomers.[18] Approaches using semiempirical potentials require phenomenological models to describe the interatomic interactions, in particular, the many-body nature of metal atom interactions. Several model potentials have been proposed and used in a number of previous investigations.[19−22] In this study, we use the semiempirical many-body Gupta potential to mimic metallic bonding.[23]

* To whom correspondence should be addressed. E-mail: posada@cifus.uson.mx (Alvaro Posada-Amarillas), Tel. +52-662-2592156.
[†] Departamento de Matemáticas, Universidad de Sonora.
[‡] Programa de Posgrado en Ciencias (Física), and Departamento de Investigación en Física, Universidad de Sonora.
[§] Departamento de Investigación en Física, Universidad de Sonora.
[||] Max Planck Institut für Festkörperforschung.
[⊥] University of Birmingham.
[#] Universidad Autónoma de San Luis Potosí.

10.1021/jp904518e CCC: $40.75
Published on Web 08/18/2009

In this paper, we give a theoretical and computer simulation perspective, performing a comprehensive analysis of the structural characteristics of 19-atom Pd/Pt clusters, considering all possible compositions. We use a genetic algorithm (GA) which incorporates the Gupta potential, as formulated by Cleri and Rosato, to explore the potential energy surface (PES) of these nanoalloys.[24,25] The 19-atom cluster is particularly interesting because the double icosahedron structure is very stable for single element clusters[26,27] and the appearance of diverse structures across the range of compositions makes it suitable for the analysis of the relationship between structure and composition. We also present a structural fingerprint for each of the predicted structures, through the simulated intensity of the X-ray diffraction pattern (XRD).[28] Clearly, a comparison of simulations and experiment is crucial in furthering our understanding of bimetallic nanoalloys, as well as for improving theoretical methods. In the future, it is expected that a more precise structural determination will be obtained by combining HRTEM and X-ray absorption spectroscopy techniques.[29]

II. Methodology

Cluster configurations were obtained by global optimization of the atom positions using the Gupta potential,[23] a semiempirical potential energy function which has proven to satisfactorily describe the interatomic bonding in late transition and noble metal clusters. This potential function is obtained from a second moment approximation to the tight-binding density of states for the *d* electrons, with parameters fitted from experimental data, such as the cohesive energy, lattice parameters, and independent elastic constants for the reference crystal structure at 0 K.[25] The Birmingham cluster genetic algorithm (BCGA) code[30] was used in the optimization process, for many initial random configurations. Typically, we carried out hundreds of optimizations for each composition in order to perform a reliable exploration of the potential energy hypersurface, focusing on Pd_nPt_{19-n} ($n = 0, \cdots, 19$) bimetallic clusters.

The BCGA code has been described previously;[19,24,30,31] thus, we give here only the parameters used in this study: population size = 40; crossover rate = 0.8; crossover type = 1-point weighted; selection = roulette; mutation rate = 0.1; mutation type = mutate_move; number of generations = 500; number of GA runs for each composition = 100. This large number of GA runs is necessary since the number of homotops depends combinatorially on the composition.[32] This vast computational effort for locating minima guarantees a high probability of finding the global minima for our 19-atom bimetallic nanoparticles. After finding the lowest energy structures, we calculated several important structural properties, including simulated XRD patterns, with the aim of quantifying structural similarities and of providing useful insights into the structural analysis of these bimetallic clusters.

III. Results and Discussion

In previous studies on Pd/Pt nanoalloys,[19] the strong dependence of the structure on composition has been demonstrated. For the 19-atom Pd/Pt nanoalloy, it was found that the double icosahedron (DI) structure appears for Pd_{19}, $Pd_{18}Pt_1$, $Pd_{17}Pt_2$, $Pd_{16}Pt_3$, and $Pd_{15}Pt_4$ (DI type I). It was also found that the lower symmetry Pt_{19} structure (Dh-Ino) is displayed by the clusters Pd_8Pt_{11}, Pd_7Pt_{12}, and for Pd_5Pt_{14} to Pd_1Pt_{18}. The Pd_6Pt_{13} cluster exhibits an hcp-type packing, corresponding to a Pt_{13}-centered anticuboctahedron capped on the six square faces by Pd atoms (hcp-type). The remaining compositions resemble the icosahedron or the DI structure, with examples including capped and waist-capped structures. The present study reproduces the former structural details, emphasizing the existence of several structural families and computing their XRD patterns. We hope that our results will provide tools for the analysis of complex energy landscapes, describing the structural patterns for these types of nanoalloys using straightforward calculations.

We have classified the nanoparticles into six structural families; for each, a representative is shown in Figure 1. It

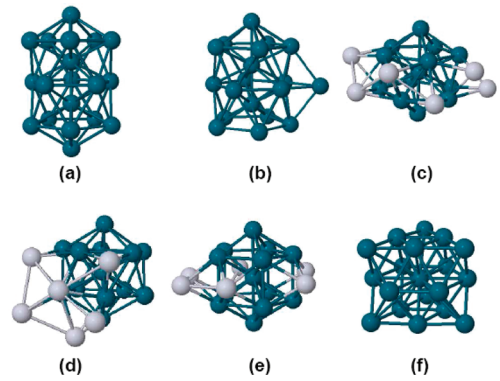

Figure 1. The ideal structures of the Pd/Pt nanoparticles obtained in this work. (a) Double icosahedron type I (DI_I). (b) Double icosahedron type II (DI_II). Icosahedron with (c) 6 adjacent equatorial faces capped (I_h-w) and (d) 4 adjacent faces capped plus 2 atoms (I_h-v). (e) Ino decahedron with equatorial faces capped (Dh-Ino). (f) The structure based on a fragment of the infinite hcp-structure.

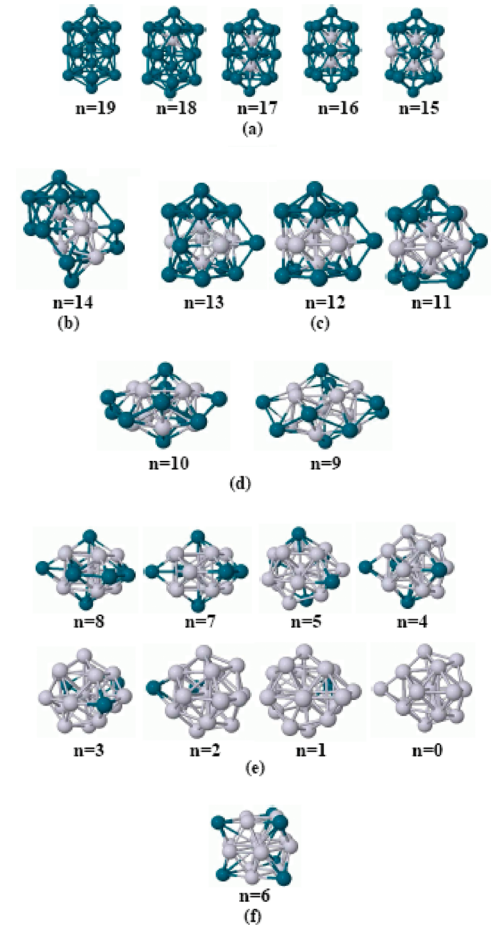

Figure 2. The structural families obtained in this study for the 19-atom Pd_nPt_{19-n} nanoparticles as a function of composition *n*. (a) DI_I structures for $n = 19$, 18, 17, 16, and 15. (b) Ih-v structure for $n = 14$. (c) DI_II structures for $n = 13$, 12, and 11. (d) Ih-w structures for $n = 10$ and 9. (e) Dh-Ino structures for $n = 8$, 7, 5, 4, 3, 2, 1, and 0. (f) The hcp-based structure for $n = 6$.

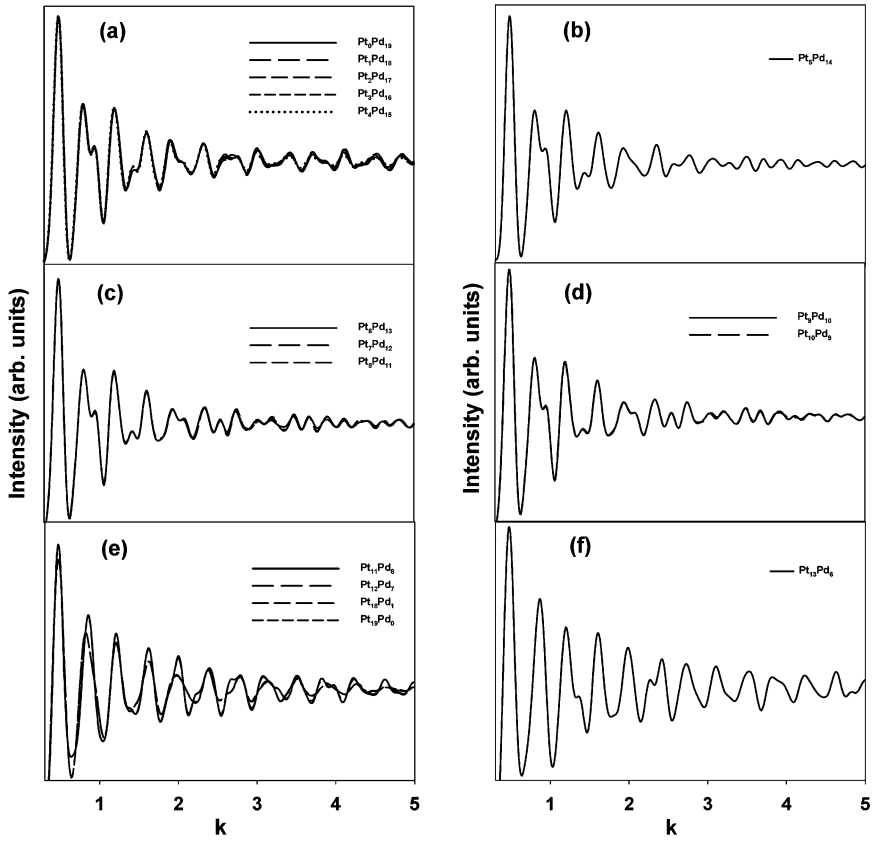

Figure 3. Simulated XRD structure factors for the structures found in this study for bimetallic 19-atom Pd_nPt_{19-n} nanoalloys. Wave vector (**k**) units are $Å^{-1}$.

TABLE 1: Geometrical Characteristics of the Structures Obtained in This Study

Pd atoms	Pt atoms	structure type	No. of Pd−Pd bonds	No. of Pt−Pt bonds	No. of Pd−Pt bonds	Pd−Pd bond length	Pt−Pt bond length	Pd−Pt bond length	average interatomic distance
19	0	DI_I	68	0	0	2.673			2.673
18	1	DI_I	56	0	12	2.698		2.583	2.677
17	2	DI_I	45	1	22	2.731	2.556	2.590	2.682
16	3	DI_I	39	3	26	2.741	2.614	2.608	2.685
15	4	DI_I	33	5	30	2.750	2.624	2.625	2.686
14	5	Ih-v	25	9	31	2.741	2.700	2.609	2.672
13	6	DI_II	21	12	33	2.776	2.693	2.618	2.682
12	7	DI_II	17	16	33	2.806	2.699	2.612	2.683
11	8	DI_II	13	19	34	2.840	2.696	2.619	2.685
10	9	Ih-w	8	21	36	2.763	2.691	2.644	2.675
9	10	Ih-w	6	25	34	2.777	2.695	2.641	2.674
8	11	Dh-Ino	2	25	34	2.658	2.659	2.635	2.646
7	12	Dh-Ino	1	29	31	2.706	2.657	2.637	2.648
6	13	hcp	0	36	24		2.666	2.609	2.643
5	14	Dh-Ino	0	38	24		2.666	2.659	2.663
4	15	Dh-Ino	0	44	18		2.672	2.644	2.649
3	16	Dh-Ino	0	50	12		2.677	2.614	2.665
2	17	Dh-Ino	0	54	8		2.673	2.614	2.665
1	18	Dh-Ino	0	58	4		2.670	2.617	2.666
0	19	Dh-Ino	0	62	0		2.668		2.668

should be noted that, apart from the hcp-based structures, all the structures have fivefold pseudosymmetry. In Figure 1a, the regular double icosahedron (DI) is labeled DI_I (DI type I). It has two internal atoms, two apex atoms, five equatorial, and two sets of five waist atoms, with 68 M−M bonds. In Figure 1b, we show the DI type II (DI_II) structure. This structure is based on the DI, but one of the apex atoms is moved to the equator, capping the two faces formed by two equatorial and two waist atoms, with 66 M−M bonds. In Figure 1c and d, we present two structures based on the regular icosahedron (I_h), one with six atoms capping six adjacent equatorial faces (I_h-w), dark atoms in Figure 1c, and another that can be described as an I_h with four atoms capping four adjacent faces, forming an irregular tetrahedron (dark atoms in Figure 1d) and two more capping faces formed by three of these and one of the original I_h (I_h-v) (Figure 1d). There are 65 M−M bonds in both clusters. The structure based on the Ino decahedron (Dh-Ino) is shown in Figure 1e, which is a Dh-Ino with five atoms capping the five equatorial faces and one more on the equator capping the faces formed by two of these and two of the original Dh-Ino, with 60 M−M bonds. Finally, in Figure 1f we show the 19-atom hcp structure, with 60 bonds. Figure 2a−f shows for $n =$

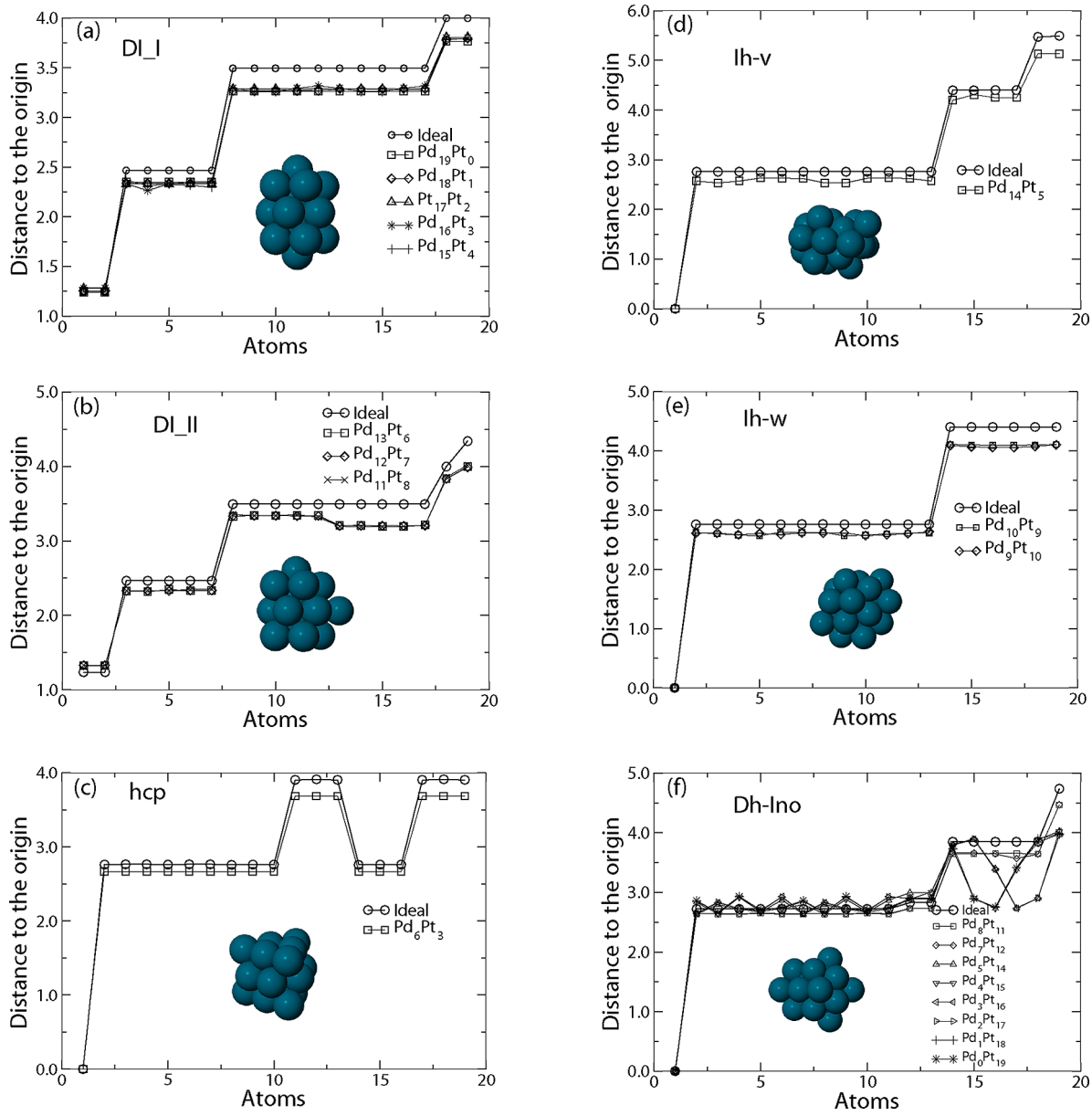

Figure 4. Radial distances (Å) of the atoms in the families of structures obtained in this study. (a) DI_I, (b) Ih-v, (c) DI_II, (d) Ih-w, (e) hcp, and (f) Dh-Ino.

0, ···, 19 the ground-state structure of the Pt_nPd_{19-n} clusters grouped into these six structural families.

Computational work is useful for analyzing the underlying structural details of this type of nanoparticles. Figure 3a−f shows the simulated XRD patterns for each of the predicted ground-state structures. There are no significant differences between those structures where the icosahedron is the basic motif (Figure 3a−d) except for k values of around 2.5 $Å^{-1}$, where peak splitting is apparent as the number of Pt atoms rises. Figure 3f corresponds to the hcp-type structure, and the plot shows a first smooth peak while a shoulder appears in the second peak. A third behavior is clearly seen in Figure 3e, corresponding to the Ino decahedron symmetry. In this figure, major differences are observed, especially in the high k value region, suggesting the existence of structural discrepancies as the composition varies. The differences in the curves of Figure 3e can be understood by analyzing Figure 2. There are two kinds of structures: one where the Ino decahedron is well-defined (Figure 2a,b), and the other where a combination of Ino decahedron and icosahedral motifs are present in the structure of the nanoalloys (Figure 2c−f). If we analyze our results from the Pt_{19} cluster structure ($n = 0$ in Figure 2e), we note that, as the number of Pd atoms rises, the structural symmetry also increases until we have a well-defined Ino decahedron ($n = 8$ in Figure 2e) as the basic structural motif.

The atomic ordering of the lowest energy configurations for the structural families found here was explored systematically, along with the radial distances of the atoms in the bimetallic nanoparticles (see Table 1 and Figure 4a−f). The structural trends of the predicted structures are similar to the ideal structures for the DI_I and hcp-type families (Figure 4a,e). ICO types I and II show an oscillatory behavior, which is more pronounced for the ICO type I structure (Figure 4b,d). The DI_II and the Ino decahedra are the structures that have evident discrepancies with respect to the ideal structures. For the DI_II structure, there is a very steep step at concentrations where the number of Pt atoms ranges from 13 to 19 (Figure 4c) and the Ino decahedron structures differ considerably from the ideal structure for practically all the concentrations where this

structure is observed, in particular, for concentrations having 14−19 Pt atoms (Figure 4f).

In Table 1, we list the number of different bonds (Pd−Pd, Pt−Pt, and Pd−Pt) in the clusters, the bond lengths, and also their average length, as well as the average interatomic distance. It can be seen that, in the Pd_nPt_{19-n} nanoparticles for $0 < n < 9$, the number of Pt−Pt bonds increases as the Pt concentration increases, but simultaneously the number of Pd−Pd bonds decreases and the number of Pt−Pd bonds increases. This means that the Pt atoms tend to aggregate together, i.e., they tend to segregate in the cluster core. For $n > 13$, there are no Pd−Pd bonds, which means that the Pd atoms tend to occupy sites that are not nearest neighbors. On the other hand, for $n = 1-2$ the Pd−Pd distance is lower than the corresponding value of the Gupta potential (2.7485 Å), although the number of Pd−Pd bonds is high. This is most likely due to the effective multiparticle interactions mediated by the Pt atoms enforced by the embedding of the Pd atoms in the Pt-rich structure. The Pt−Pt and Pt−Pd distances are also lower than the respective Gupta potential parameters (2.7747 Å and 2.76 Å, respectively) for all values of n.

IV. Conclusions

We have obtained a composition-dependent structural description of 19-atom Pd/Pt nanoparticles using a GA global search method to find the lowest energy structures, for all possible compositions. A comprehensive analysis of the morphology is presented, along with structural information giving details on the atomic ordering and the interatomic distances for both the ideal structural motifs and the predicted structures. We found that for Pd-rich compositions the Pt atoms tend to segregate, increasing the number of Pd−Pt bonds. However, for Pd-rich clusters, the Pd atoms tend to be separated. We also observe that from composition Pd_9Pt_{10} to Pd_{19} the icosahedral geometry is dominant over the decahedron-type structures. The simulated XRD patterns present characteristic behavior and structural discrepancies for the Dh-Ino nanoalloys, revealing that an increase in the number of Pd atoms in the range $n = 0-8$ produces higher symmetry structures. The interatomic distances in the predicted structures are generally smaller than those of the corresponding ideal structure (Table 1 and Figure 4), except for the Dh-Ino structure. Recent theoretical studies have shown that the energetic distribution of minima may change when higher-level theoretical tools are used,[33] which suggests that future work must be carried out using quantum chemistry methods, such as DFT, in order to verify the predicted ground-state structures and the structural families obtained using semiempirical Gupta (or other) potentials.

Acknowledgment. A.P.A. acknowledges CONACyT for financial support through project 24060. R.P.C. is also grateful to CONACyT for the award of a PhD scholarship. J.M.M.C. acknowledges financial support from CONACyT through grant no. 50650 and partial financial support from PIFI (México) through grant 2007-24-21.

References and Notes

(1) Templeton, A. C.; Wuelfing, W. P.; Murray, R. W. *Acc. Chem. Res.* **2000**, *33*, 27. Elghanian, R.; Storhoff, J. J.; Mucic, R. C.; Letsinger, R. L.; Mirkin, C. A. *Science* **1997**, *277*, 1078.

(2) Rousset, J. L.; Cadrot, A. M.; Cadete Santos Aires, F. J.; Renouprez, A.; Mélinon, P.; Perez, A.; Pellarin, M.; Vialle, J. L.; Boyer, M. *J. Chem. Phys.* **1995**, *102*, 8574.

(3) Ferrando, R.; Jellinek, J.; Johnston, R. L. *Chem. Rev.* **2008**, *108*, 845.

(4) Coq, B.; Figueras, F. *J. Mol. Catal. A* **2001**, *173*, 117.

(5) Ching, S.-H.; Hoffman, A.; Guslienko, K.; Bader, S. D.; Liu, C.; Kay, B.; Makowski, L.; Chen, L. *J. Appl. Phys.* **2005**, *97*, 10R101.

(6) Joswig, J.; Seifert, G.; Niehaus, T. A.; Springborg, M. *J. Phys. Chem. B* **2003**, *107*, 2897. Rooney, P.; Rezaee, A.; Xu, S.; Manifar, T.; Hassanzadeh, A.; Podoprygorina, G.; Böhmer, V.; Rangan, C.; Mittler, S. *Phys. Rev. B* **2008**, *77*, 235446.

(7) J. Gavnholt, J.; Schiøtz, J. *Phys. Rev. B* **2008**, *77*, 035404. Toshima, N.; Yonezawa, T. *New J. Chem.* **1998**, *21*, 1179.

(8) Kobayashi, H.; Yamauchi, M.; Kitagawa, H.; Kubota, Y.; Kato, K.; Takata, M. *J. Am. Chem. Soc.* **2008**, *130*, 1818.

(9) Sounderya, N.; Zhang, Y. *Recent Patents on Biomedical Engineering* **2008**, *1*, 34.

(10) Burda, C.; Chen, X.; Narayanan, R.; El-Sayed, M. A. *Chem. Rev.* **2005**, *105*, 1025.

(11) Toshima, N.; Yonezawa, T. *New J. Chem.* **1998**, *22*, 1179.

(12) Alayoglu, S.; Nilekar, A. U.; Mavrikakis, M.; Eichhorn, B. *Nat. Mater.* **2008**, *7*, 333.

(13) Bazin, D.; Triconnet, A.; Moureaux, P. *Nucl. Instrum. Methods B* **1995**, *97*, 41. Bazin, D.; Mottet, C.; Treglia, G. *Appl. Catal., A* **2000**, *200*, 47. Wu, M.-L.; Chen, D.-H.; Huang, T.-Ch. *Langmuir* **2001**, *17*, 3877.

(14) Calvo, F. *Faraday Discuss.* **2008**, *138*, 75. Cheng, D.; Huang, S.; Wang, W. *Chem. Phys.* **2006**, *330*, 423.

(15) Bazin, D.; Guillaume, D.; Pichon, Ch.; Uzio, D.; Lopez, S. *Oil Gas Sci. Technol.* **2005**, *60*, 801.

(16) Stanislaus, A.; Cooper, B. H. *Catal. Rev.-Sci. Eng.* **1994**, *36*, 75.

(17) Balleto, F.; Ferrando, R. *Rev. Mod. Phys.* **2005**, *77*, 371, and references therein.

(18) Paz-Borbón, L. O.; Johnston, R. L.; Barcaro, G.; Fortunelli, A. *J. Chem. Phys.* **2008**, *128*, 134517. Paz-Borbón, L. O.; Johnston, R. L.; Barcaro, G.; Fortunelli, A. *J. Phys. Chem. C* **2007**, *111*, 2936. Díaz-Ortiz, A.; Aguilera-Granja, F.; Michaelian, K.; Berlanga-Ramírez, E. O.; Montejano-Carrizales, J. M.; Vega, A. *Physica B* **2005**, *370*, 200.

(19) Lloyd, L. D.; Johnston, R. L.; Salhi, S.; Wilson, N. T. *J. Mater. Chem.* **2004**, *14*, 1691.

(20) Michaelian, K.; Garzón, I. L. *Eur. Phys. J. D* **2005**, *34*, 183.

(21) Paz-Borbón, L. O.; Mortimer-Jones, T. V.; Johnston, R. L.; Posada-Amarillas, A.; Barcaro, G.; Fortunelli, A. *Phys. Chem. Chem. Phys.* **2007**, *9*, 5202.

(22) Cheng, D.; Huang, S.; Wang, W. *Chem. Phys.* **2006**, *330*, 423.

(23) Gupta, R. P. *Phys. Rev. B* **1981**, *23*, 6265.

(24) Johnston, R. L.; Roberts, C. *Cluster Geometry Optimization Genetic Algorithm Program*, University of Birmingham, 1999; Roberts, C. Genetic Algorithms for Cluster Optimization, PhD Thesis, University of Birmingham, 2001; Johnston, R. L. *J. Chem. Soc., Dalton Trans.* **2003**, 4193.

(25) Cleri, F.; Rosato, V. *Phys. Rev. B* **1993**, *48*, 22.

(26) Jadzinsky, P. D.; Calero, G.; Ackerson, C. J.; Bushnell, D. A.; Kornberg, R. D. *Science* **2007**, *318*, 430.

(27) Manninen, K.; Akola, J.; Manninen, M. *Phys. Rev. B* **2003**, *68*, 235412.

(28) Koga, K.; Takeo, H.; Ikeda, T.; Ohshima, K. *Phys. Rev. B* **1998**, *57*, 4053.

(29) Park, J.; Joo, J.; Kwon, S. G.; Jang, Y.; Hyeon, T. *Angew. Chem., Int. Ed.* **2007**, *46*, 4630.

(30) Johnston, R. L. *Dalton Trans.* **2003**, 4193.

(31) Massen, C.; Mortimer-Jones, T. V.; Johnston, R. L. *J. Chem. Soc., Dalton Trans.* **2002**, 4375.

(32) Jellinek J.; Krissinel, E. B. *Theory of Atomic and Molecular Clusters*; Springer: Berlin, 1999.

(33) Ferrando, R.; Fortunelli, A.; Johnston, R. L. *Phys. Chem. Chem. Phys.* **2008**, *10*, 640.

JP904518E